Numerical Prediction of Various Cavitation Erosion Mechanisms

Article *in* Journal of Fluids Engineering · October 2019

DOI: 10.1115/1.4045365

4 authors:

Ignacijo Biluš
University of Maribor
29 PUBLICATIONS **289** CITATIONS
SEE PROFILE

Marko Hočevar
University of Ljubljana, Faculty of Mechanical Engineering
124 PUBLICATIONS **1,214** CITATIONS
SEE PROFILE

Matevz Dular
University of Ljubljana
107 PUBLICATIONS **2,520** CITATIONS
SEE PROFILE

Luka Lešnik
University of Maribor
17 PUBLICATIONS **239** CITATIONS
SEE PROFILE

1.1 Paper title
Numerical prediction of various cavitation erosion mechanisms

1.2 Authors info
Ignacijo Biluš[1], ignacijo.bilus@um.si,
Marko Hočevar[2], marko.hocevar@fs.uni-lj.si,
Matevž Dular[2] matevz.dular@fs.uni-lj.si (corresponding author),
Luka Lešnik[1] luka.lesnik@um.si.

[1] Laboratory for Turbine Machinery, Faculty of Mechanical Engineering, University of Maribor, Smetanova ulica 17, 2000 Maribor, Slovenia,
[2]Laboratory for Water and Turbine Machines, Faculty of Mechanical Engineering, University of Ljubljana, Aškerčeva 6, 1000 Ljubljana, Slovenia.

1.3 Abstract
Numerical prediction of cavitation erosion is a great scientific and technological challenge. In the past many attempts were made - many successful. One of the issues when a comparison between a simulation and erosion experiments is made, is the great difference in time scale. In the present work we do not attempt to obtain quantitatively accurate predictions of erosion process but concentrate qualitatively on cavitation mechanisms with quantitative prediction of pressure pulses which lead to erosion. This is possible, because of our recent experimental work on simultaneous observation of cavitating flow and cavitation erosion by high speed cameras. In this study the numerical simulation was used to predict details of the cavitation process during the vapour collapse phase. The fully compressible, cavitating flow simulations were performed to resolve the formation of the pressure waves at cavitation collapse. We tried to visualize the mechanisms and dynamics of vapour structures during collapse phase at the Venturi geometry. The obtained results show that unsteady RANS simulation of cavitation is capable of reproducing 4 out of 5 mechanisms of cavitation erosion, found during experimental work.

KEY WORDS: Computational Fluid Dynamics, Caviation, Erosion, Prediction

1.4 Paper text
INTRODUCTION

Cavitation is the phenomenon that consists of the formation, activity and collapse of vapor structures inside a liquid medium. Usually, the phenomenon is undesired, since it causes many negative effects. Among negative effects, the cavitation erosion is the most complex one, since it combines complicated

hydrodynamics with solid material response at the mechanical and metallurgical perspective. The pioneer work on the erosive potential of cavitation was performed by Rayleigh [1]. The work is based on single bubble dynamics analysis. A wide range of researchers tried to clarify the bubble dynamics problem and understand the cavitation phenomena since then [2], [3]. The numerous experimental studies were done where single bubble [4], [5] and multi bubble structures (clouds) collapse were analyzed [7]–[9].

In the last years, several effective CFD methods were also developed to numerically simulate, analyze and predict complicated multiphase flow phenomena and cavitation [10]–[16]. Comparing to the experiments, the numeric provides more information about dynamics and allows deeper insight in the mechanisms of vapor bubbles during their collapse. The numerical study performed by T. J.C. Van Terwisga et al. [17] reviews physical mechanisms for cavitation erosion loads and post processing procedure for the assessment of the risk of cavitation erosion. The fundamental work done on cavitation erosion by Bark et al. [18] suggests that collapse energy is occurring in the form of large scale eddies which take place in the breakup region of sheet cavitation. The same research focuses on the question whether the conditions for erosive cavitation can be predicted from an URANS method, without the necessity to compute the details of the actual collapse. Li et al. [19] presented new erosion intensity function and applied it on the case unsteady cavitating flow over an NACA0015 hydrofoil using URANS method. Johnsen and Colonius [20] numerically simulated the shock-induced collapse of a single gas bubble in shockwave lithotripsy. The lithotripter pulse is modeled as a compressive shock front of constant amplitude while the wall pressure is considered as an indication of potential damage. Similarly, B. Budich et al [21] performed a qualitative comparison of cavitating flow aggressiveness at the model propeller VP1304 by the maximum pressure criterion. The analysis was further extended using collapse detection algorithm (i.e. statistical method) for analysis of collapse locations, rates and intensity.

The erosion risk models, that can be used in conjunction with a multiphase URANS solver were compared in latest study of Melissaris et al [22]. The results show reasonable agreement with experiment and strong potential of further research and optimization.

Currently the general consensus is that the formation of the damage is a result of a consequence of events - an approach termed “the energy cascade” [18]. Interestingly, the events themselves are not satisfactorily explained yet. The reason for this could be the fact, that he problem is ubiquitous, as it occurs on many scales, both in space and in time. The understanding is, that the collapse of the cavitation cloud causes a shock wave which interacts with single cavitation bubbles that are present in the vicinity of the wall. These then collapse and cause damage. There are still many opened questions, which were addressed in our previous works:

- How exactly a cloud collapses [23], [24]?
- How a single bubble collapses and causes erosion [25]?
- How does a pit form [26]?
- Can we predict the damage [27]–[29]?

Many studies were made to pursue the above questions from the simulation point of view. Peters et al. [30] presented numerical modelling and prediction of cavitation erosion on ship propellers. The implicit, pressure-based approach using the RANS equations was used to describe the turbulent cavitating flow for the case of propeller in full scale and model scale. Solver was coupled with a microscopic erosion model that is based on the microjet hypothesis presented by Dular et al. They defined that a numerical erosion impact on a face supposedly occurs, when vapour condition and damage condition were fulfilled. In same study, the prediction of cavitation erosion was validated using experimental data for the model scale propeller also. Mottyll & Skoda [14] used a density based solver to simulate cavitating flows. Collapses of vapour clouds are predicted based on identification of individual cells in which divergence of velocity field changes its sign. For the assessment of erosion process, two different statistical methods i.e. erosion probability and collapse detector are utilized. The model was verified on the case of ultrasonic horn and using ASTM G32-10 erosion test. While many researchers still build on URANS approach, other moved to LES. An exemplary study on erosion prediction in small geometries, was published by Koukouvinis et al. [31]. Recently, Schenke et al. [32] introduced an interesting approach to the understanding and prediction

of the aggressiveness of the collapsing cavitating structures by an energy conservative method, although it was not yet rigorously supported by the experiments.

But, as experimental techniques progress, novel questions and challenges arise. The present paper is a logical next step to the work of Wang et al. [29] where we have shown the capability of CFD to predict the general dynamics of cavitation erosion – comparing simulations to our experiments [6]. Since the experiment was considerably improved since then, this contribution investigates the capability of CFD to predict more details of the erosion process. We performed fully compressible, cavitating flow simulations to resolve the formation of the shock waves during cavitation collapse phase which is directly related to the formation of the damage in the vicinity of the solid material surfaces.

We have confirmed that cavitation cloud shedding causes different typical hydrodynamic mechanisms and results in extreme conditions which are connected with material erosion. The results are valuable for further numerical investigation and development of cavitation erosion prediction models.

GEOMETRY AND CAVITATION DYNAMICS

The results of simulations are compared against the experiments performed by Dular et al [6]. This section gives only a brief overview. Further details on the experimental methodology can be found in [6].

The investigated geometry is a 10 mm wide Venturi section with an 18° converging and 8° diverging angles (Fig. 1). The throat dimensions are $10\times10\text{mm}^2$.

The operating conditions were set to 490000 Pa (absolute pressure) and 27.4 m/s, which was achieved in about 0.05 s after opening the valve (a transient startup was needed as the foil gets extensive coverage by cavitation pits in an order of 1 second of exposure to cavitation).

In the study [6] we discuss the 5 different hydrodynamic phenomena that lead to the formation of the pit (Fig. 2). Here we only briefly introduce them.

Figure 2 shows a schematic representation of the results, which we obtained during our experimental campaigns, [6]. The most significant feature, which, in fact, defines the state of developed cavitation is cavitation cloud shedding. We can follow this process from the attached cavity (A), which grows (B) and,

at some point, reaches its maximal size - at this moment a stagnation point forms at its closure (C). This is the first instant and position where cavitation damage was found - the combination of local pressure increase (stagnation pressure) and small bubble structures that are shed from the cavity closure form a plausible environment for bubble collapse and erosion occurrence. Moving on, the reentrant jet enters the attached cavity (D) and causes a cloud separation (E). At this point also, the occurrence of damage was observed - similarly as before, a combination of bubble presence and slight increase of pressure (stagnation) causes conditions for damage occurrence. The cloud is then carried by the flow (F and G) and it implodes in a higher-pressure region downstream. The implosion results in a pressure wave that triggers further damage (H). Experiments also showed that the cloud can manifest in different shapes – spherical collapse (H) is actually very rare compared to the horseshoe (L) and twister (O) clouds. The side wall effects cause a roll-up of the cloud, which takes a distinctive horseshoe shape. When it is carried downstream, it splits at the top and the remaining legs collapse - focusing the bubbles towards the wall. The twister cloud (O) has the same origin as the horseshoe cloud. The main difference is that the spanwise vortex remains liquid just downstream of the attached cavity. Due to the existence of the slip velocity between the vapor and liquid phase, it catches up with the previously shed cloud and focuses the bubbles towards the wall. In the presented paper, we will try to predict the described mechanisms of cavitation erosion using time dependent numerical simulation.

NUMERICAL PROCEDURE

Governing equations

The used governing equations were based on the conservation form of the Reynolds averaged Navier-Stokes (RANS) equations. The first equation is continuity equation, which can be written as:

$$\frac{\partial}{\partial t}\rho_m + \frac{\partial}{\partial x_i}(\rho_m \overline{u_i}) = 0 \qquad (1)$$

The equation (2) presents the equation for conservation of momentum:

$$\frac{\partial}{\partial t}(\rho_m \bar{u}_i) + \frac{\partial}{\partial x_j}(\rho_m \bar{u}_i \bar{u}_j)$$

$$= -\frac{\partial}{\partial x_i} p + \frac{\partial}{\partial x_j}\left[(\mu_m + \mu_t)\left(\frac{\partial \bar{u}_i}{\partial x_j} + \frac{\partial \bar{u}_j}{\partial x_i} - \frac{2}{3}\delta_{ij}\frac{\partial \overline{u_k}}{\partial x_k}\right)\right] \quad (2)$$

The third is the energy equation which can be written as:

$$\frac{\partial}{\partial t}(\rho_m E) + \nabla \cdot [\vec{u}(\rho_m E + p)] = \nabla \cdot \left(k_{eff} \nabla T\right) \quad (3)$$

where p denotes the pressure, u is the velocity, μ and μ_t are laminar and turbulent viscosity and δ_{ij} is the Kronecker delta function. Energy E is calculated as $E = h - \frac{p}{\rho_m} + \frac{u^2}{2}$, k_{eff} is the effective conductivity. The energy equation was used to include the influence of density change on pressure field, while cavitation flow was considered as isothermal [33].

The mixture density and viscosity are defined as a homogeneous mixture function of liquid phase and vapor phase volume fraction:

$$\rho_m = \rho_v \alpha_v + \rho_l (1 - \alpha_v) \quad (4)$$

$$\mu_m = \mu_v \alpha_v + \mu_l (1 - \alpha_v) \quad (5)$$

where α is the volume fraction and subscripts m, l and v indicate mixture, liquid and vapor phases.

Turbulence model

Numerical modeling of turbulent flow is very complex process in which turbulence model play a significant role. It is used for calculation of fluctuating part of pressure and velocity in RANS equations. The appropriate turbulence model must be applied in order to accurately predict cavitation inception and detachment of the cavity from solid surface. The standard $k - \varepsilon$ model, commonly used in computational fluid dynamics, is over-estimating the eddy viscosity in mixture region and excessively attenuates the cavitation instability. This makes it unsuitable for numerical prediction of cavitation phase detachment from solid surface. Coutier-Delgosha et al. [13] proposed modified $RNG\ k - \varepsilon$ model, which used Re-

normalization group for effective viscosity calculation. Using this it can reduce the overestimated eddy viscosity of $k-\varepsilon$ turbulence model by employing the turbulent viscosity μ_t as:

$$\mu_t = f(\rho_m) C_\mu \frac{k^2}{\varepsilon} \tag{6}$$

$$f(\rho_m) = \rho_v + \frac{(\rho_m - \rho_v)^n}{(\rho_l - \rho_v)^{n-1}} \tag{7}$$

where we define the coefficient $C_\mu = 0.09$ according to $k-\varepsilon$ model and $n = 10$ as proposed in [13].

Cavitation model

The liquid-vapor mass transfer is governed by the vapor mass transport equation as:

$$\frac{\partial}{\partial t}(\alpha\rho_v) + \nabla \cdot (\alpha\rho_v \overrightarrow{u_v}) = R_e - R_c \tag{8}$$

where R_e and R_c denotes liquid phase evaporation and vapor phase condensation source terms.

Interphase mass transfer rates were calculated using Zwart-Gerber-Belamri cavitation model [34]:

$$R_e = F_{vap} \frac{3\alpha_{nuc}(1-\alpha_v)\rho_v}{R_B} \sqrt{\frac{2}{3}\frac{p_v - p}{\rho_l}} \tag{9}$$

$$R_c = F_{cond} \frac{3\alpha_v \rho_v}{R_B} \sqrt{\frac{2}{3}\frac{p - p_v}{\rho_l}} \tag{10}$$

Based on our previous experience [29, 35], and comparison performed by Morgut et al. [36], used cavitation model proved with a precise cavitation predicting capability and a good convergence behavior. The evaporation is initiated at nucleation sites when pressure p is lower than vaporization pressure $p < R_c$; the condensation occurs when pressure is higher than vaporization pressure $p > p_v$. In the equations (9) and (10) F_{vap} and F_{cond} are the empirical calibration coefficients of evaporation and condensation, α_{nuc} is the nucleation site volume fraction and R_B is the nucleation site radius. In the presented paper the recommended values of presented coefficients were used [29]. They are: $F_{vap} = 50$, $F_{cond} = 0.01$, $\alpha_{nuc} = 5 \cdot 10^{-4}$ and $R_B = 2 \cdot 10^{-6}$. The vaporization pressure was set on $p_v = 3574\ Pa$.

In order to reproduce complex flow mechanisms associated with cavitation, the compressibility of the flow has to be taken into account. The variations in liquid phase density ρ_l were calculated using Tait equation as:

$$\rho_l = \rho_{ref} \sqrt[n]{\frac{p+B}{p_{ref}+B}} \tag{11}$$

where ρ_{ref} and p_{ref} denote the reference liquid density and pressure. The values of constants $n = 7$ and $B = 300MPa$ were selected for water. The vapor fraction obeyed the ideal gas law.

Speed of sound (c) of a bubbly mixture depends mainly on the local void fraction (α) (Brennen [37]):

$$c = \left[\frac{\alpha}{\gamma \cdot p}(\rho_l(1-\alpha) + \rho_v \alpha)\right]^{-\frac{1}{2}} \tag{12}$$

where p is the local presure and (γ) is the politropic index (in the present case we assume isentropic process). Shamsborhan et al. [38] tested the influence of void fraction and the influence of the coefficient of compressibility of the fluid on speed of sound. They compared experimental results to several different models which also consider the compressibility of vapor and liquid phase. According to this, we assume that the accuracy of speed of sound prediction is in the same range of accuracy of the models tested by Shamsborhan et al.

Simulation setup

The commercial CFD program "ANSYS-Fluent" was used for numerical simulation of the RANS equation system. A mass flow rate of water and static pressure values were prescribed on the inlet and outlet boundary respectively, strictly following the experimental data.

A no-slip wall was applied on the Venturi walls surface with standard wall function. The convergence criteria were set to 1×10^{-4}. The simulations were initialized by running the calculation under upwind scheme based on COUPLED algorithm for four shedding periods until a time-periodic solution has been reached, with a time step of 1.6×10^{-4} s. Afterwards, the algorithm was changed to the second-order scheme and additionally, the time step was reduced to only 2×10^{-7} s to obtain a more precise resolution concerning to

the cavity shedding off and collapse.

Mesh

In order to obtain good accuracy and convergence structural hexahedral grid was generated to model fluid flow and cavitation inception in our model, Fig. 3. The model was divided in two sections, the nozzle section and the Venturi test section.

As can be seen on Fig. 3 more refined mesh was used in Venturi test section.

Estimation of numerical error

Before analyzing the cavitation regimes, a through grid independence analysis was carried out using the grid convergence index (GCI). The Grid Convergence Index (GCI) provides a uniform measure of convergence for grid refinement studies [39]. It is based on estimated fractional error derived from the generalization of Richardson extrapolation [40]. The GCI value represents the resolution level and how much the solution approaches the asymptotic value.

In order to evaluate the grid independence and to calculate the CGI we monitored the velocity and turbulence kinetic energy values at domain outlet on three hexa structured meshes, generated using ANSYS-ICEM CFD. The mesh independence study for the steady flow example is summarized in the Tab. 1. Following the results of this analysis, the discretization uncertainty was calculated [40]. The grid convergence index presenting the calculated uncertainty was less than 4% for fine mesh and less than 5% for medium mesh. In order to assure minimal discretization error, the fine mesh was used for further analysis. At used mesh, the Y+ value at Venturi surface was in the range of 20. Following the study of Wang et al [29] this mesh density provided satisfactory average cavity shedding frequency, cavity length and the average longest attached cavity comparing to the experiment.

RESULTS

In this study we do not focus on the integral and quantitative prediction of the cavitation damage, but rather on the investigation of the capability of qualitative reproduction of cavitation mechanisms with quantitative prediction of pressure pulses, which were observed during our experimental campaign.

Typical features from Fig. 2 where we observed cavitation erosion [24] are noted with detailed view of Venturi test section at Fig. 4, with isosurface of vapour volume fraction $\alpha_v = 20\%$.

In the following sections we will focus on four events where we observed erosion experimentally and evaluate the capability of a widely used CFD tool to predict it.

Closure of the attached cavity pocket

Closure of the attached cavity pocket occurs when the cavity cloud stops to grow. Figure 5 shows the results of the simulation, depicting the rapid increase of the pressure at the cavity closure line. The upper sequence shows the contours of vapor fraction, and the lower sequence the corresponding pressure field on the surface of the Venturi. The highest pressure emerges at reference time t = 0 μs (d). Frames are taken from 0.6 μs prior to pressure peak (a), to 0.4 μs after the peak (f). Please also see the corresponding diagram in Fig. 6.

We concentrate our observation to the attached cavity closure region. As the cavity ceases to grow and begins to retract, the flow over the cavity turns towards the surface (due to the pressure difference) what causes the formation of a stagnation point. The pressure rises from nearly vapor pressure to a stagnation pressure (please see the Fig. 2c). The flow then separates into a stream that follows the main flow direction and the jet that penetrates the cavity (Fig. 2d), The latter then flows upstream and eventually causes cloud separation (Fig. 2e). At the stagnation point a somewhat higher pressure causes the collapse of smaller cavities which are shed from the main attached structure. These collapse violently and cause pressure peaks in the range of MPa - high enough pressure to initiate further collapses down the energy cascade (cloud collapse - bubble collapse [18], [41], [42]) and cause erosion.

The formation of the more pronounced stagnation point and the consequent increase in pressure can also nicely be seen a diagram in Fig. 6 - the pressure was monitored at a point, which at the beginning lies inside the attached cavity and is later wetted as the cavity retracts.

We see that the pressure is close to the vapor pressure at the beginning of the monitoring. At the moment the cavity retracts, at t=0 μs, it increases rapidly to roughly 5 bar (absolute). This corresponds well to the stagnation pressure $p = \frac{\rho v^2}{2}$. Of course, this pressure is much lower than the yield stress of the material (even for the thin aluminum foil, which was used in the present experiments). But one needs to consider that very small cavitation structures - single bubbles, which are impossible to capture by this type of simulation, are shed from the closure line. These will undergo a violent collapse as they enter the stagnation zone, which will result in either shock wave or microjet formation - and these phenomena are aggressive enough to damage material.

Separation of cavitation cloud

The separation of cavitation cloud occurs when an upstream flow of water cuts the attached cavity into two parts. At this point, a very local and rapid increase of pressure in the region between the attached and separated cavity can be observed, Fig 7. The collapse occurs at reference time t = 0 μs (e). Frames are taken from 1.4 μs prior to collapse (a), to 0.4 μs after the collapse (f). Please also see the corresponding diagram in Fig. 8.

The re-entrant jet that penetrated the attached cavity flows upstream until it loses momentum. At this point it turns up and causes the separation of cavitation cloud. In the separation region again, a stagnation point momentarily forms - the following dynamics is similar to the one at the cavity closure line with one significant difference. The cavity closure region is relatively stable, the local pressure there corresponds to the stagnation pressure ($p = \frac{\rho v^2}{2}$). On the other hand, at cavitation cloud separation the stagnation point forms instantly, hence, for a brief time, much more severe water hammer pressure conditions prevail - $p =$

ρvc. These are more aggressive and can cause more damage during the consequent cascade of evens that lead to erosion.

The same can be observed quantitatively as it is shown in the diagram in Fig. 8.

As a consequence of interaction between the reentrant jet that "cuts" into the main flow, a water hammer conditions form very shortly after the cloud separates. The local pressure at the surface of the Venturi rapidly rises and reaches 10 bar. At these conditions the unresolved bubble structures in the region will collapse violently and cause erosion to the material.

Spherical cavitation cloud collapse

The separated cloud of bubbles can take on different shapes. One of them is close to a spherical one and is known to collapse coherently. A sequence in Fig. 9 shows such a collapse and the corresponding pressure field at the surface of the Venturi. The collapse occurs at reference time t = 0 μs (e). Frames are taken from 4.2 μs prior to collapse (a), to 1 μs after the collapse (f). Please also see the corresponding diagram in Fig. 10.

The cloud collapse occurs at a certain distance from the surface. Due to the nature of the cavitation model, there can be no bubbles present in the region between the collapse point and the surface of the Venturi (vapor almost instantaneously condensates in a high pressure region, see Eqn. 10). Hence the emitted pressure wave traverses the distance with the sonic velocity which equals the one in pure water (~1500 m/s) and reaches the surface of the Venturi shortly after. The assumption of the wave traveling with the sound speed is in the accordance with previous experimental works (Vogel et al. [43]), where it was found that it is supersonic for only a fraction of the length of the time step of the present simulation (in the order of 100 ns in the case of a collapse of a perfectly spherical unbounded cavity). The progression of the shock wave can be seen in the image (e) as it spreads in a spherical manner through the domain.

Again, we can observe the same phenomenon in a qualitative manner. The diagram in Fig. 10 shows the time evolution of pressure at the surface just beneath the cloud. Frame (a) from Fig. 9 lies outside the diagram at -4.2 μs, frame (b) is at -3 μs.

As the shock wave reaches the surface, the pressure rises rapidly to 10 bar and enables conditions at which single cavitation bubbles or very small cavitation structures (both unresolved in the present simulation) collapse and cause material erosion.

Horseshoe cavitation cloud collapse

Another, very distinctive manifestation of cavitation cloud is the so-called horseshoe structure. Its collapse begins at its center and moves towards the arms. Sequence in Fig. 11 shows the process. The pressure peak emerges at reference time t = 0 μs. The right arm of the horseshoe collapses much sooner than the left one. In order to present it well the frame (a) is taken 8 μs and frame (b) 4 μs before the main cavity collapse (frame (e) at 0 μs). Frame (c) is at t=-3 μs. The last frame (f) is at 2.6 μs. Please also see the corresponding diagram in Fig. 12.

We see that the collapse begins at the center, the right arm of horseshoe collapses first, followed by the left arm shortly after. The second collapse is more intensive, likely due to the interaction with the shock wave emitted at the collapse of the right arm. The increase of the pressure at the surface occurs later, again the time delay corresponds perfectly to the shock wave transition time. Later on, the wave spreads spherically over the domain (as in the case of spherical cloud collapse).

The same can be concluded form the pressure evolution at the surface of the Venturi (Fig. 12).

First, we observe the increase of pressure to about 9 bar, this can be attributed to the collapse of the right arm of the horseshoe. About 3 μs later the left arm collapses, what causes a significantly more pronounced pressure peak (14 bar) as the one from the right arm collapse. The horseshoe type of collapse is also known to be one of the most aggressive types of collapse [18] [24]. This is, as our simulation suggests, due to the

interaction between the shock wave emitted from the collapse of the first arm with the remaining bubbles contained in the second arm.

Twister cavitation cloud collapse

The twister type of collapse is still not directly experimentally confirmed. Our previous experiments suggest that the mechanism is the interaction between the liquid vortex and the spherical bubble cloud. For it to form, the liquid vortex needs to move slightly faster than the cloud - this was recently shown by Khlifa et al. [44]. As the vortex catches the bubble cloud it forms a horseshoe type structure which collapses in the same manner as the "normal" horseshoe cloud. To be able to capture this numerically one would need to consider solving N-S equations for each fluid separately and not to resolve to the homogeneous approach as in the present approach. This is one of the tasks we intend to pursue in the future.

Further comparison

We noted on several occasion that the simulation is unable to capture the small cavitation structures. Also, the predicted pressure peaks are much too low to cause damage to an engineering material. On the other hand, the order of magnitude of predicted pressure peaks is correct comparing to experiments performed by Reisman et al [45] and Ganesh et al [46].

In general, cavitation erosion is a result of a cascade of events [18], [24], [41]. Collapse of the macroscopic cavitation structure triggers a collapse of a single bubble, which collapses in a spherical of micro-jet manner. Such a collapse is much more potent, and the local pressures can exceed the yield strength of the material. Nevertheless, we have shown previously that the "driving pressure", the one we have predicted in the present simulation, can be relatively well corelated to the measured damage [24]. In Figure 13 we show the CFD predicted maximal pressure from individual type of event together with the average measured damage on the same geometry and at same operating conditions [24].

One can see that the simulation is obviously able to capture the correct correlation and the order of aggressiveness of individual events (cavity closure, cloud separation, spherical and horseshoe type cloud collapses).

CONCLUSIONS

The purpose of the present study was to evaluate the capability of numerical simulation to capture details of the cavitating flow which are directly related to cavitation erosion. Up until now, studies dealt mainly with statistical comparisons - comparison of numerical results against long term erosion measurements. In the present study, we used our previous unique results, where we could observe cavitating flow and the simultaneous erosion process at a time resolution of 1/30000s.

A fully compressible cavitating flow was considered in simulations. This way we were able to capture the formation of the shock waves during cavitation collapse phase - these are believed to be directly related to the formation of damage.

We were able to capture 4 processes (stagnation point at cavity closure, process at cloud separation, spherical and horseshoe cloud collapse) by the present simulation. Since we used a homogeneous fluid flow approach, we could not predict the slip velocity between the phases and the twister cloud collapse, which is governed by this process.

We show that it is currently possible to predict most of the features of cavitating flow, which eventually lead to erosion. Even more - the trends of the numerical predictions are correct - although we cannot speak about quantitative agreement - due to the space and time resolution of the simulation we did not (could not) predict the high-pressure shocks, which are emitted at a small structure collapses and are directly related to material damage.

The majority of simulations of cavitating flow put emphasis on the correct modelling of turbulence but many times neglect the highly compressible nature of two phase flow. Also, none to very little attention is usually given to the origin and dynamics of various cavitation structures, which can be related to different erosion mechanisms. In the present study we focused on this void and have shown that a fully compressible

simulation, associated with the correct prediction of cavitation structure topology, is needed when one wants to predict the regions, which a prone to be damaged by the cavitation bubble collapses. For the first time the simulation was compared against advanced, time resolved measurements of cavitation erosion, which is an important step towards the derivation of an universal cavitation erosion model in the future.

LIST OF SYMBOLS

C_μ	coefficient
E	specific energy
F_{vap}	vaporisation coefficient
F_{cond}	condensation coefficient
h	enthalpy
k_{eff}	effective conductivity
k	turbulence kinetic energy
p_v	vaporisation pressure
p	pressure
R_B	nucleation site radius
R_e	evaporation source term
R_c	condensation term
u	velocity
α	volume fraction
α_{nuc}	nucleation site volume fraction
δ_{ij}	Kronecker delta function
ε	dissipation
μ	viscosity

μ_t turbulent viscosity

μ_m viscosity of homogeneous mixture

ρ_m density of homogeneous mixture

ρ density

ACKNOWLEDGMENTS

The authors acknowledge the financial support from the Slovenian Research Agency (research core Funding No. P2-0401, and Projects No. J2—6774)

1.5 References

[1] Lord Rayleigh, F. R. S., 1917, "VIII. On the pressure developed in a liquid during the collapse of a spherical cavity," The London, Edinburgh, and Dublin Philosophical Magazine and Journal of Science, vol. 34, no. 200, pp. 94–98.

[2] Plesset, M. S., Chapman, R. B., 1971, "Collapse of an initially spherical vapour cavity in the neighbourhood of a solid boundary," Journal of Fluid Mechanics, vol. 47, no. 2, pp. 283–290.

[3] Franc, J. P., 2017 "The Rayleigh-Plesset equation: a simple and powerful tool to understand various aspects of cavitation," Fluid Dynamics of Cavitation and Cavitating Turbopumps. L. d'Agostino, M. V. Salvetti, eds. Springer, Vienna, pp. 1–42.

[4] Isselin, J. C., Alloncle, A. P., Autric, M. 1998, "On laser induced single bubble near a solid boundary: Contribution to the understanding of erosion phenomena," Journal of Applied Physics, vol. 84, no. 10, pp. 5766–5771.

[5] Sagar, H. J., Hanke, S., Underberg, M., Feng, C., el Moctar, O., Kaiser, S. A. 2018, "Experimental and Numerical Investigation of Damage on an Aluminum Surface by Single-Bubble Cavitation," Materials Performance and Characterization, vol. 7, no. 5, pp. 985–1003.

[6] Dular, M., Petkovšek, M., 2015, "On the mechanisms of cavitation erosion – combining high speed videos to damage patterns," Experimental Thermal and Fluid Science, vol. 68, pp. 359–370.

[7] Hansson, I., Kedrinskii, V., Morch, K. A., 1982, “On the dynamics of cavity clusters,” Journal of Physics D: Applied Physics, vol. 15, no. 9, pp. 1725–1734.

[8] Biluš, I., Bombek, G., Hočevar, M., Širok, B., Cenčič, T., 2014, “The Experimental Analysis of Cavitating Structure Fluctuations and Pressure Pulsations in the Cavitation Station,” Strojniški vestnik – Journal of Mechanical Engineering, vol. 60, no. 3, pp. 147–157.

[9] Biluš, I., Bizjan, B., Lešnik, L., Širok, B., Pečnik, B., Dular, M., 2017, “Non-contact method for analysis of cavitating flows,” Ultrasonics, vol. 81, pp. 178–186.

[10] Gomboc, T., Zadravec, M., Iljaž, J., Sagadin, G., Hriberšek, M., 2019, “Numerical model of three stage spray drying for zeolite 4A - water suspensions coupled with CFD flow field”, International journal of simulation modelling, vol. 18, no. 2, pp. 217–228.

[11] Dular, M., Bachert, R., Stoffel, B., Širok, B., 2005, “Experimental evaluation of numerical simulation of cavitating flow around hydrofoil,” European Journal of Mechanics, B/Fluids, vol. 24, no. 4, pp. 522–538.

[12] Znidarcic, A., Coutier-Delgosha, O., Marquillie, M., Dular, M., 2015, “An algorithm for fast DNS cavitating flows simulations using homogeneous mixture approach,” Journal of Physics: Conference Series, vol. 656, no. 1, pp.1–4.

[13] Coutier-Delgosha, O., Fortes-Patella, R., Reboud, J. L., 2003, “Evaluation of the Turbulence Model Influence on the Numerical Simulations of Unsteady Cavitation,” Journal of Fluids Engineering, vol. 125, no. 1, p. 38–45.

[14] Mottyll, S., Skoda, R., 2016, “Numerical 3D flow simulation of ultrasonic horns with attached cavitation structures and assessment of flow aggressiveness and cavitation erosion sensitive wall zones,” Ultrasonics Sonochemistry, vol. 31, pp. 570–589.

[15] Morgut, M., Jošt, D., Škerlavaj, A., Nobile, E., Contento, G., 2018, “Numerical predictions of cavitating flow around a marine propeller and kaplan turbine runner with calibrated cavitation models,” Strojniski Vestnik/Journal of Mechanical Engineering, vol. 64, no. 9, pp. 543–554.

[16] Bilus, I., Morgut, M., Nobile, E., 2013, “Simulation of sheet and cloud cavitation with homogenous

transport models," International Journal of Simulation Modelling, vol. 12, no. 2, pp. 94–106.

[17] Van Terwisga, T. J. C., Fitzsimmons, P. A., Foeth, E. J , Li, Z., 2009, "Cavitation Erosion: A critical review of physical mechanisms and erosion risk models," Proceedings of the 7th International Symposium on Cavitation, Ann Arbor, MI, August 16-20, 2009, Paper No. 41, pp. 1–13.

[18] Bark, J. T., Friesch, G., Kuiper, J., Ligtelijn, G., 2004, "Cavitation Erosion on Ship Propellers and Rudders," 9th Symposium on Practical Design of Ships and Other Floating Structures, Luebeck-Travemuende Germany, September 12-17, 2004, pp. 554–561.

[19] Li, Z., Pourquie, M., van Terwisga, T. J. C, 2014, "Assessment of Cavitation Erosion With a URANS Method," Journal of Fluids Engineering, vol. 136, no. 4, pp. 041101-1–041101-11.

[20] Johnsen, E., Colonius, T., 2008, "Shock-induced collapse of a gas bubble in shockwave lithotripsy, " The Journal of the Acoustical Society of America, vol. 124, no. 4, pp. 2011–2020.

[21] Budich, B., Borrmann, F., Schmidt, S. J., Adams, N. A., 2015, "Assessment of Erosion Aggressiveness for the Cavitating Model Propeller VP1304 by Fully Compressible Numerical Simulation," Proceedings of 18th Numerical Towing Tank Symposium, NuTTS 2015, Marstrand, Sweden, September 28-30, 2015, pp. 1–6.

[22] Melissaris, T., Bulten, N., van Terwisga, T. J. C, 2019, "On the Applicability of Cavitation Erosion Risk Models with a URANS Solver," Journal of Fluids Engineering, vol. 141, no. 10, pp. 101104-1–101104-15.

[23] Petkovšek, M., Dular, M., 2013, "Simultaneous observation of cavitation structures and cavitation erosion," Wear, vol. 300, no. 1–2, pp. 55–64.

[24] Dular, M., Petkovšek, M., 2015, "On the mechanisms of cavitation erosion - Coupling high speed videos to damage patterns," Experimental Thermal and Fluid Science, vol. 68, pp. 359–370.

[25] Dular, M., Pozar, T., Zevnik, J., Petkovšek, R., 2019, "High speed observation of damage created by a collapse of a single cavitation bubble," Wear, vol. 418-419, pp. 13–23.

[26] Dular, M., Coutier-Delgosha, O., Petkovšek, M., 2013, "Observations of cavitation erosion pit formation," Ultrasonics Sonochemistry, vol. 20, no. 4, pp. 1113–1120.

[27] Dular, M., Coutier-Delgosha, O., 2009, "Numerical modelling of cavitation erosion," Proceedings of the ASME Fluids Engineering Division Summer Conference, FEDSM 2008, Jacksonville, Florida August 10–14, 2008, vol. 2, pp.15–22.

[28] Dular, M., Coutier-Delgosha, O., 2009, "Numerical modelling of cavitation erosion," International Journal for Numerical Methods in Fluids, vol. 61, no. 12, pp. 1388–1410.

[29] Wang, J., Petkovšek, M., Houlin, L., Širok, B., Dular, M., 2015, "Combined numerical and experimental investigation of the cavitation erosion process," Journal of Fluids Engineering, vol. 137, no. 5, pp. 051302-1–051302-9.

[30] Peters, A., Lantermann, U., el Moctar, O., 2018, "Numerical prediction of cavitation erosion on a ship propeller in model- and full-scale," Wear, vol. 408–409, pp. 1–12.

[31] Koukouvinis, P., Gavaises, M., Li, J., Wang, L., 2016, "Large Eddy Simulation of Diesel injector including cavitation effects and correlation to erosion damage," Fuel, vol. 175, pp. 26–39.

[32] Schenke, S., van Terwisga, T. J. C., 2019, "An energy conservative method to predict the erosive aggressiveness of collapsing cavitating structures and cavitating flows from numerical simulations," International Journal of Multiphase Flow, vol. 111, pp. 200–218.

[33] Petkovšek, M., Dular, M., 2017, "Observing the thermodynamic effects in cavitating flow by IR thermography," Experimental thermal and fluid science, vol. 88, pp. 450–460.

[34] Zwart, P., Gerber, A., Belamri, T., 2004, "A Two-Phase Flow Model for Predicting Cavitation Dynamics", Proceedings of the 5th International Conference on Multiphase Flow, ICMF 2004 Jokohama, Japan, May 30 - June 4, 2004, pp. 152.

[35] Morgut, M., Nobile, E., Biluš, I., 2011, "Comparison of mass transfer models for the numerical prediction of sheet cavitation around a hydrofoil," International Journal of Multiphase Flow, Volume 37, no. 6, pp. 620–626.

[36] Morgut, M., Nobile, E., 2012, "Numerical Predictions of Cavitating Flow around Model Scale Propellers by CFD and Advanced Model Calibration," International Journal of Rotating Machinery, Volume 2012, pp. 618180-1–618180-11.

[37] Brennen, C. E., 1995, “Cavitation and Bubble Dynamics,” Oxford University Press, London.

[38] Shamsborhan, H., Coutier-Delgosha, O., Caignaert, G., Nour, F. A., 2010, “Experimental determination of the speed of sound in cavitating flows,” Experiments in Fluids, vol. 49, no. 6, pp. 1359–1373.

[39] Roache, P. K., 1994, “Perspective: A Method for Uniform Reporting of Grid Refinement Studies,” Journal of Fluids Engineering, vol. 116, no. 3, pp. 405–413.

[40] Celik, I. B., Ghia, U., Roache, P. J., Freitas, C. J., H. Coleman, Read, P. E., 2008, “Procedure for Estimation and Reporting of Uncertainty Due to Discretization in CFD Applications,” Journal of Fluids Engineering, vol. 130, no. 7, pp. 78001-1–78001-4.

[41] Fortes-Patella, R., Reboud, J. L., Briancon-Marjollet, L., 2004, “A phenomenological and numerical model for scaling the flow aggressiveness in cavitation erosion,” Cavitation erosion Workshop, Val de Reuil, France, May 27-28, 2004, pp. 1–36.

[42] Dular, M., Bachert, B., Stoffel, B., Širok, B., 2004, “Relationship between cavitation structures and cavitation damage,” Wear, vol. 257, no. 11, pp.1176–1184.

[43] Vogel, A., Busch, S., 1996, “Shock wave emission and cavitation bubble generation by picosecond and nanosecond optical breakdown in water," The Journal of the Acoustical Society of America, vol. 100, no. 1, pp. 148–165.

[44] Khlifa, I., Vabre, A., Hočevar, M., Fezzaa, K., Fuzier, S., Roussette, O., Coutier-Delgosha, O., 2017, “Fast X-ray imaging of cavitating flows,” Experiments in Fluids, vol. 58, p. 157-1–157-22.

[45] Reisman, G. E., Wang, Y. C., Brennen, C. E., 1998, “Observations od shock waves in cloud cavitation,” Journal of Fluid Mechanics, vol. 355, pp. 255–283.

[46] Ganesh, H., Makiharju, S. A., Ceccio, S. L., 2017, “Bubbly shock propagation as a mechanism of shedding in separated cavitatning flows,” Journal of Hydrodynamics, vol. 29, no. 6, pp. 907–916.

1.6 Table caption list

Tab. 1: Mesh independence study.

1.7. Figure caption list

Fig. 1: The Venturi geometry and the test-section [6].
Fig. 2: Schematic representation of observed mechanisms that lead to occurrence of cavitation erosion. The instants of damage appearance are denoted by the darker color. An arrow marks the region where the pits occur [6].
Fig. 3: Computational domain and detail of the mesh.
Fig. 4: Typical locations and instances of damage occurrence as given by the present simulation.
Fig. 5: Numerically predicted cavitation dynamics and pressure evolution at its closure.
Fig. 6: Pressure evolution at the cavity closure line as a function of time.
Fig. 7: Experimentally observed and numerically predicted cavitation dynamics at cavitation cloud separation.
Fig. 8: Pressure evolution in the region of cloud separation as a function of time.
Fig. 9: Experimentally observed and numerically predicted spherical cavitation cloud collapse.
Fig. 10: Measures and numerically predicted damage evolution at spherical cavitation cloud collapse.
Fig. 11: Experimentally observed and numerically predicted horseshoe cavitation cloud collapse.
Fig. 12: Measures and numerically predicted damage evolution at horseshoe cavitation cloud collapse.
Fig. 13: Comparison between the predicted maximal local pressure and the measured damage from our past work [24].

1.8 Table

Tab. 1: Mesh independence study.

Mesh	Number of nodes	Velocity [m/s]	Turbulence kinetic energy [J/kg]
Coarse (1)	243745	9.469	2.605
Medium (2)	602982	9.413	2.645
Fine (3)	1393133	9.374	2.616
GCI_{fine} [%]	-	1.94	3.73
GCI_{medium} [%]	-	2.46	4.68

1.9 Figures

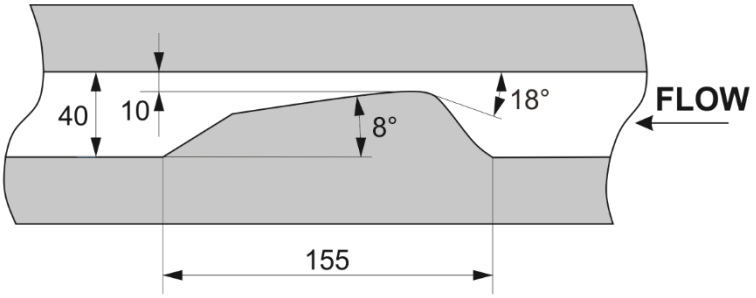

Fig. 1: The Venturi geometry and the test-section [6].

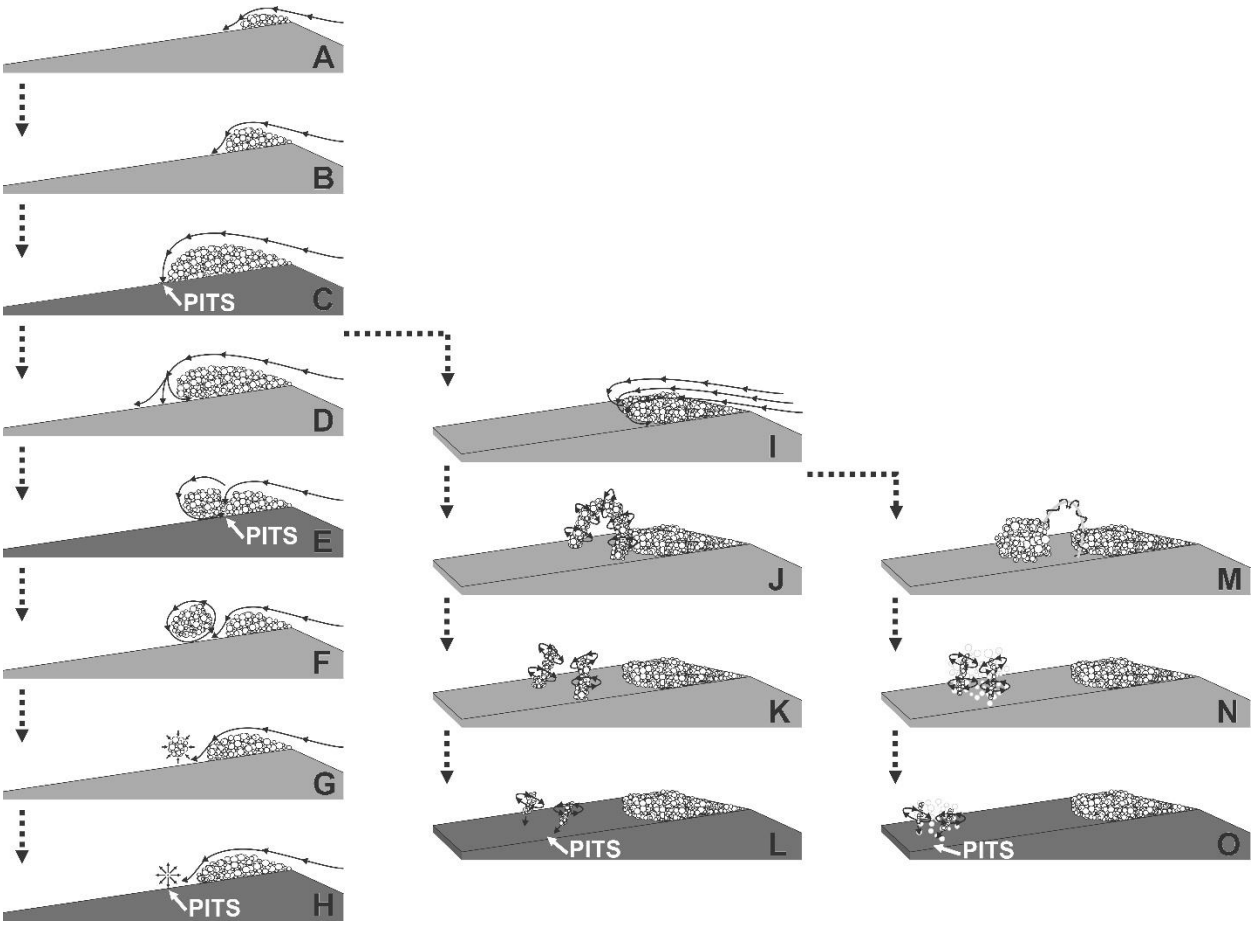

Fig. 2: Schematic representation of observed mechanisms that lead to occurrence of cavitation erosion. The instants of damage appearance are denoted by the darker color. An arrow marks the region where the pits occur [6].

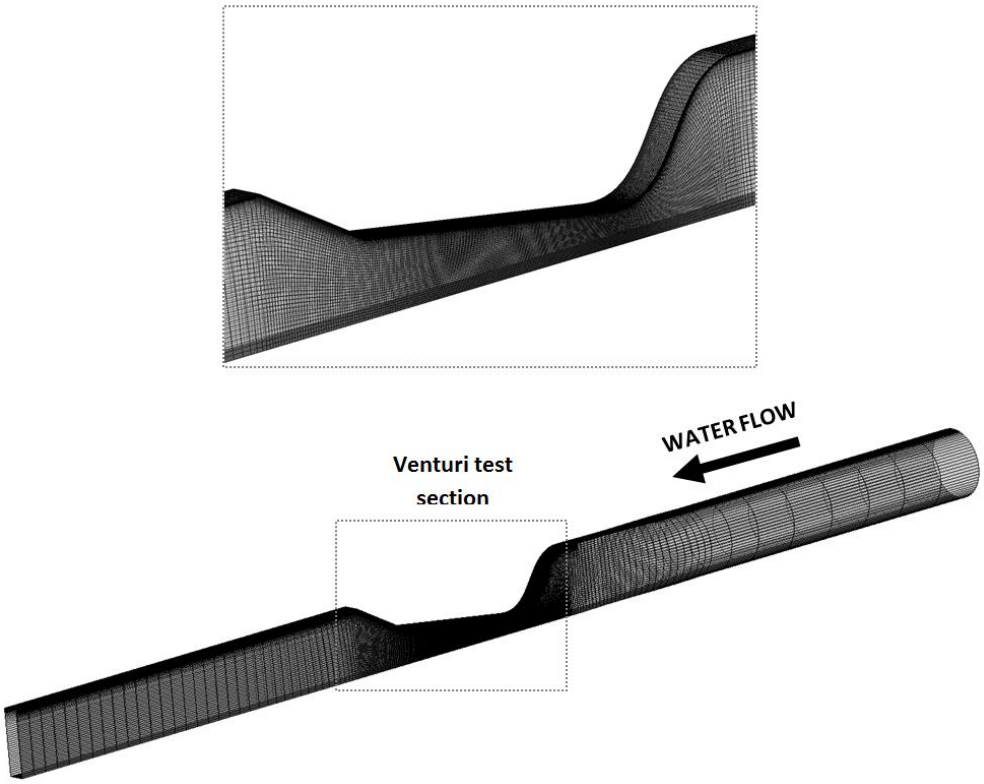

Fig. 3: Computational domain and detail of the mesh.

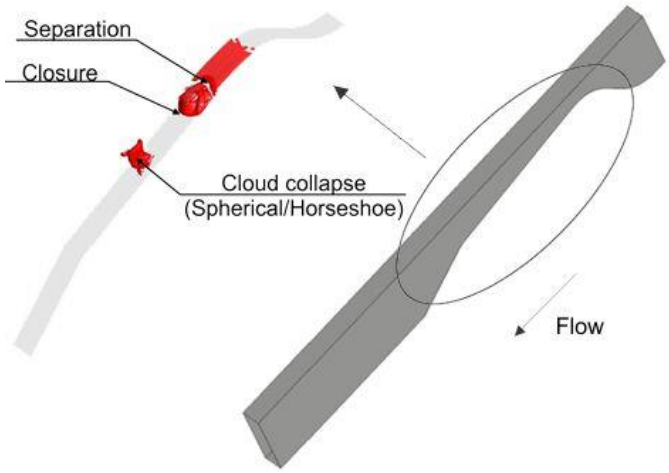

Fig. 4: Typical locations and instances of damage occurrence as given by the present simulation.

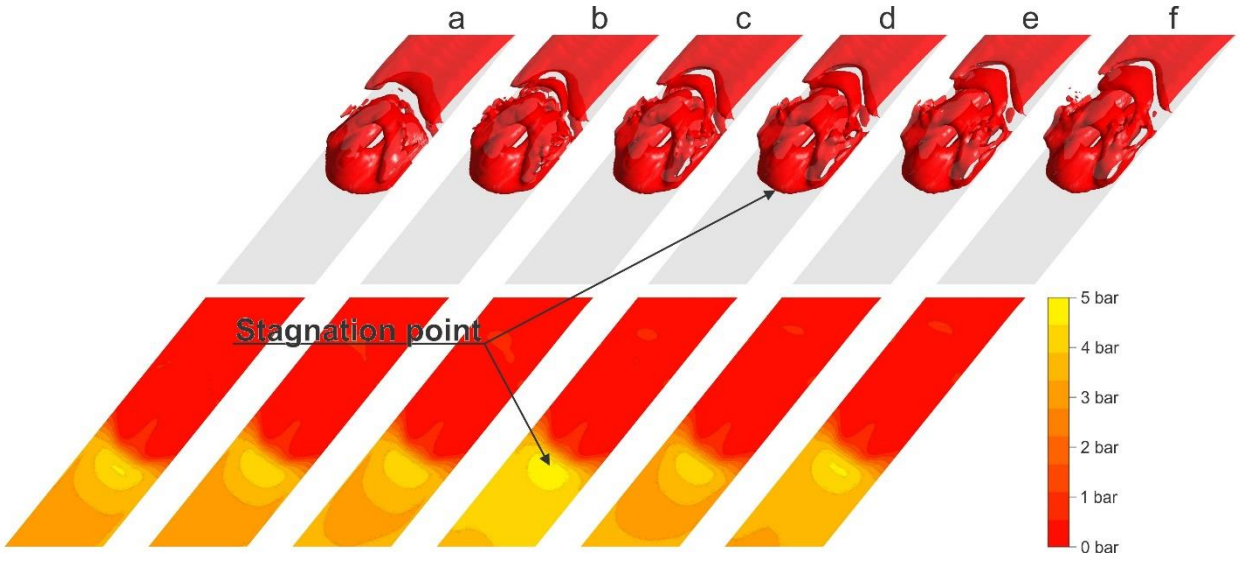

Fig. 5: Numerically predicted cavitation dynamics and pressure evolution at its closure.

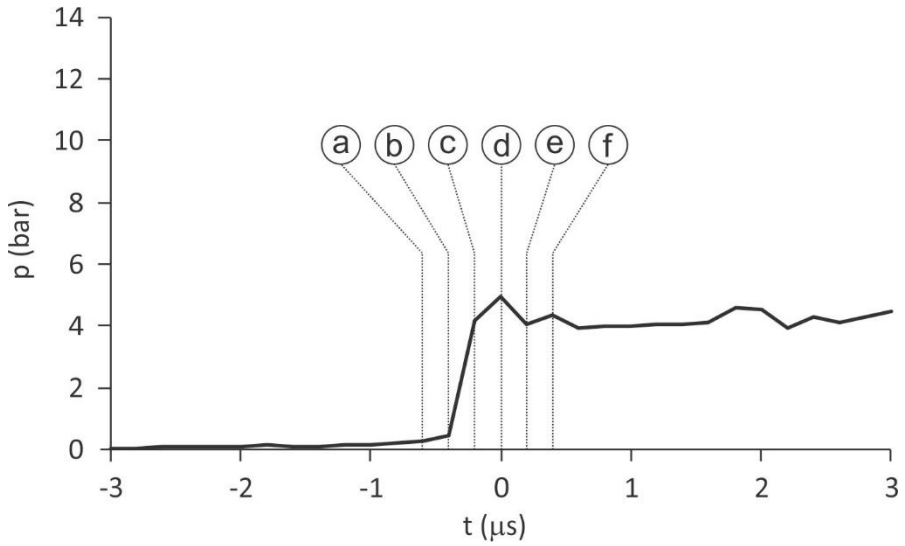

Fig. 6: Pressure evolution at the cavity closure line as a function of time.

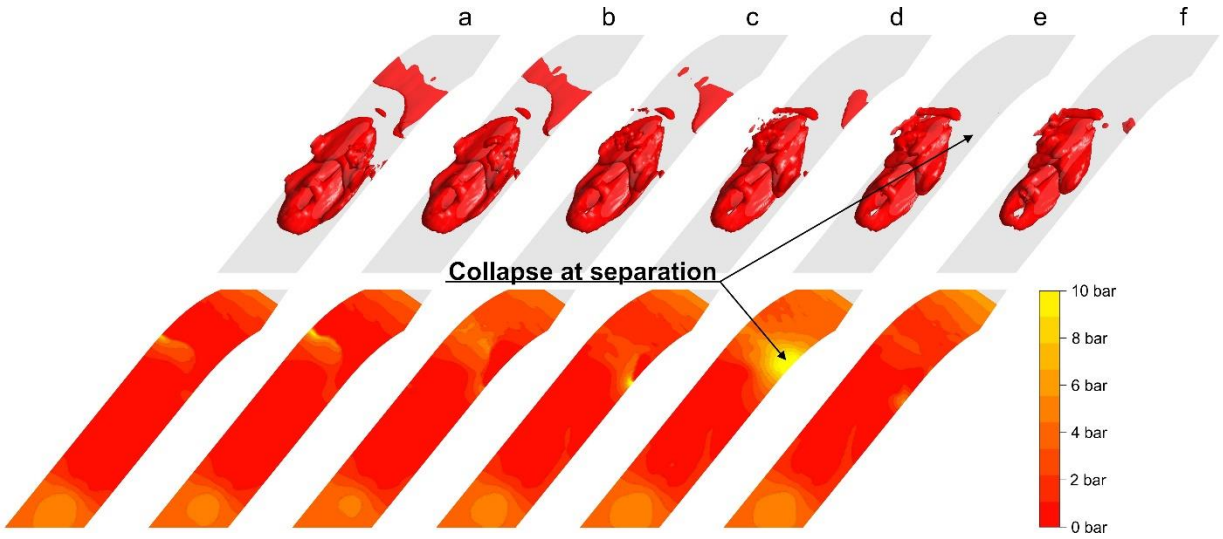

Fig. 7: Experimentally observed and numerically predicted cavitation dynamics at cavitation cloud separation.

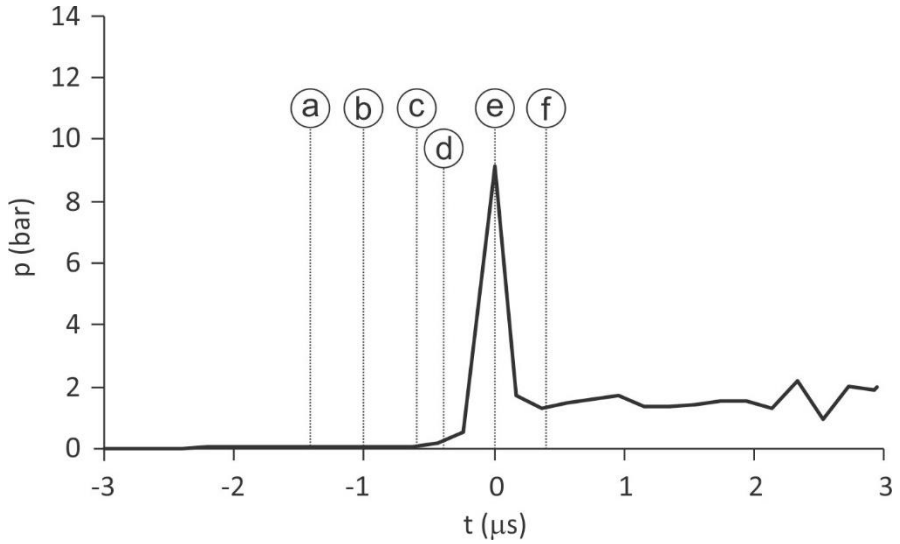

Fig. 8: Pressure evolution in the region of cloud separation as a function of time.

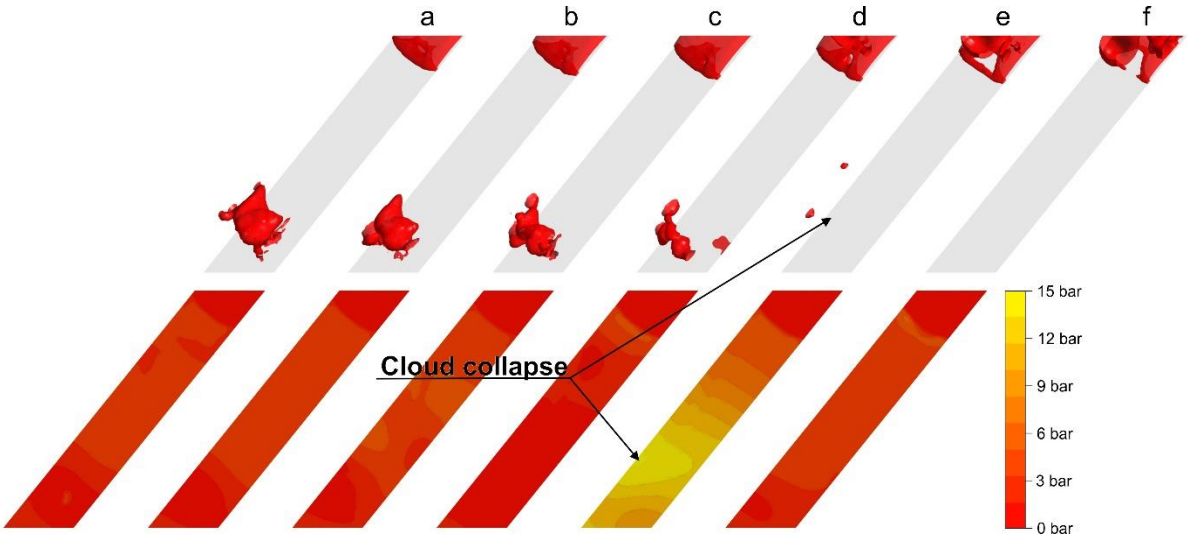

Fig. 9: Experimentally observed and numerically predicted spherical cavitation cloud collapse.

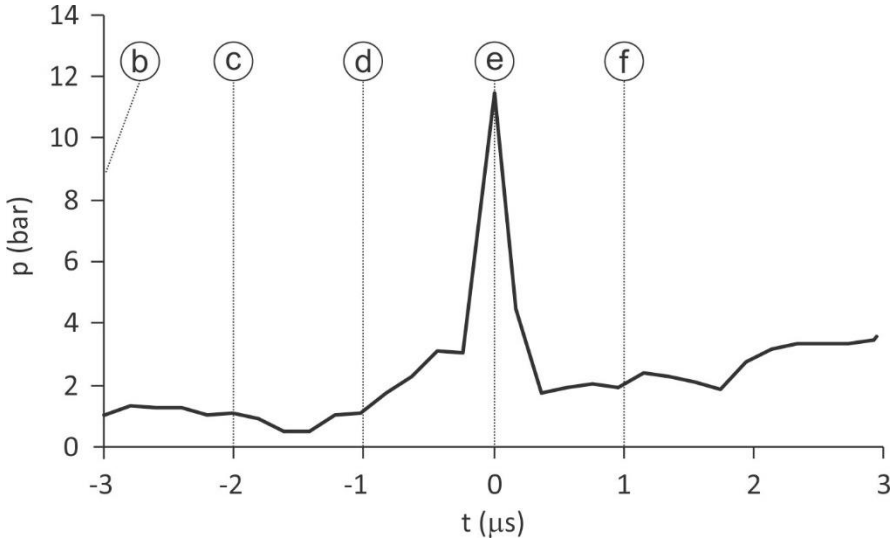

Fig. 10: Measures and numerically predicted damage evolution at spherical cavitation cloud collapse.

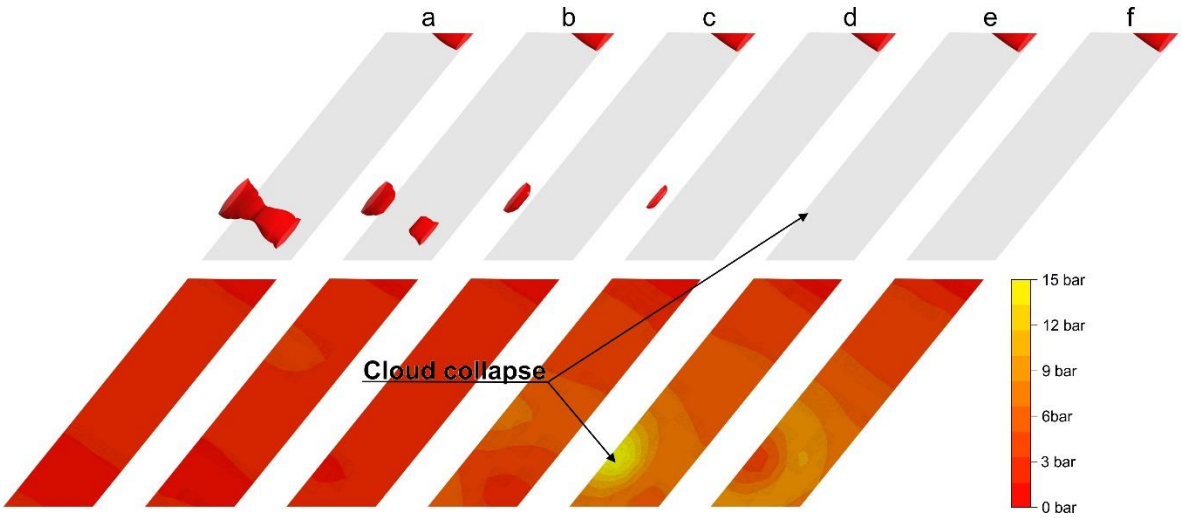

Fig. 11: Experimentally observed and numerically predicted horseshoe cavitation cloud collapse.

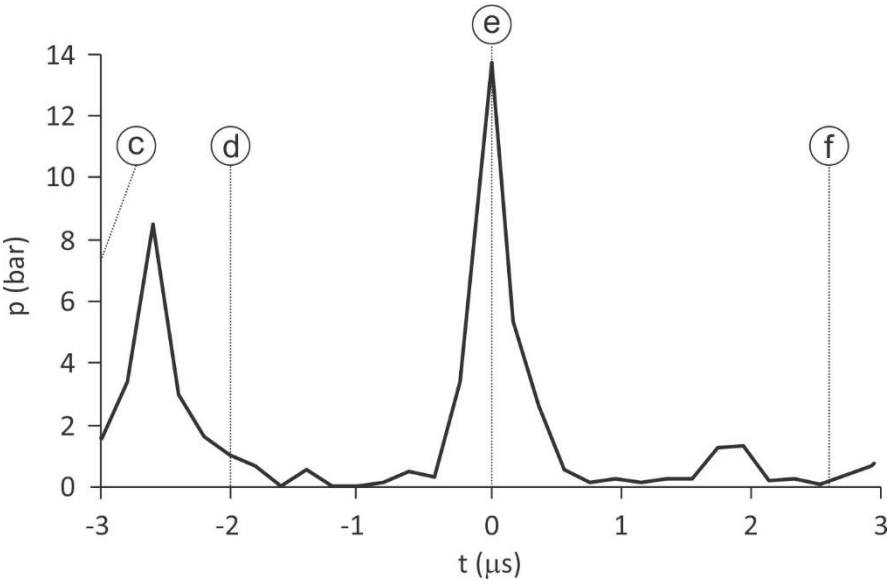

Fig. 12: Measures and numerically predicted damage evolution at horseshoe cavitation cloud collapse.

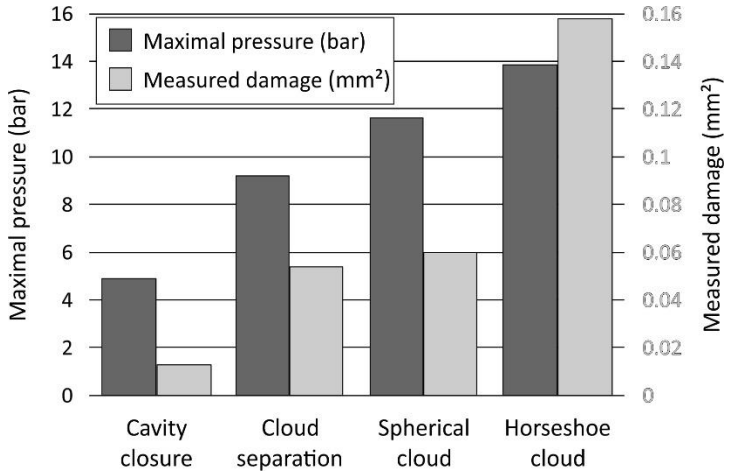

Fig. 13: Comparison between the predicted maximal local pressure and the measured damage from our past work [24].